TRI-PP-89-89
Oct 1989

Muonium production from fine silica powder

A.C. Janissen,* G.A. Beer, G.R. Mason, and A. Olin†
University of Victoria, Victoria, British Columbia, Canada V8W 2Y2

T.M. Huber§ and A.R. Kunselman
University of Wyoming, Laramie, Wyoming 82071

T. Bowen and P.G. Halverson**
University of Arizona, Tucson, Arizona 85721

C.A. Fry‡
University of Rochester, Rochester, New York 14627

K.R. Kendall†† and G.M. Marshall
TRIUMF, Vancouver, British Columbia, Canada V6T 2A3

J.B. Warren§§
University of British Columbia, Vancouver, British Columbia, Canada V6T 1W5

Abstract

The muonium atom, μ^+e^- , is a simple system from which to gain information about the e-μ interaction both to test the existing theory of QED and to search for physics beyond the standard model. A systematic study has been carried out of the production and properties of thermal muonium from a fine silica powder. The velocity and angular distributions are examined, as well as the experimental conditions resulting in the optimum production rate. The particular properties of silica powder which give it its muonium-producing capability are investigated. These studies are carried out in the context of a diffusion model, the validity of which is examined.

(submitted to Physical Review A)

I. INTRODUCTION

A. Motivation

The muonium atom, μ^+e^- , is formed in the final stage of the process whereby a positive muon loses its energy through interactions with matter, and is often the state in which the μ^+thermalizes. Being the simplest bound state of an electron and a muon, muonium is an interesting system from which to gain information about the e - μ interaction.[1] In particular, measurement of the hyperfine structure[2,3] provides a sensitive test of QED. The muonium Lamb shift[4,5] and 1S–2S transition[6] have been measured with less precision. The μ^+e^- system is also a convenient place to look for the effects of new interactions such as the lepton number violating process of muonium conversion to antimuonium, μ^-e^+ .[7,8]

The technique described in this work for producing muonium was developed to facilitate this conversion measurement. In this paper, we report a more detailed study of this phenomenon in order to establish a model of the process which is valid over a range of production target conditions.

In the first observation of muonium by Hughes *et al.*,[9] polarized muons were stopped in a target of argon gas at 50 atmospheres pressure, and identification was made by observing the characteristic Larmor precession frequency of muonium. Although this technique produced a large yield of muonium, $(85 \pm 9)\%$ of incident muons,[10] it was recognized that for some experiments muonium would have to be observed in vacuum. For example, muonium to antimuonium conversion is suppressed by collisions with gas atoms. Similarly, measurements of the muonium Lamb shift are also done in vacuum since gas collisions de-excite the 2S state.

In order to produce muonium in vacuum, a beam-foil method was developed[11,12] where a low-energy muon beam was passed through a thin foil of metal, typically gold or aluminum. This technique has a relatively low muonium yield, 0.03% of incoming muons, and the muonium which is produced is moving with epithermal velocities of approximately 0.01 times the speed of light.

Production of muonium with thermal velocities was attempted by Kendall[13] who studied muonium diffusing out of hot tungsten and platinum foils. Positive results were obtained but duplicating them proved difficult. Mills *et al.*[14] studied hot W foils and report a muonium yield of $(4 \pm 2)\%$ of the stopped muons. These results, also, have been difficult to duplicate since the technique is sensitive to the cleanliness of the W surface. Foils heated to 2800 K provide a difficult environment for many types of apparatus.

B. Formation of muonium in fumed silica

Muonium production has been studied from a fine powder of fumed silica[15,16] manufactured under the trade name Cab-O-Sil.[17] The muonium produced travels with thermal velocities, hence the atoms travel only ~2 cm in a muon lifetime. This compact source enables experiments, such as the search for antimuonium conversion or the 1S-2S transition energy measurement, to examine the entire muonium cloud instead of sampling a portion of it.

Cab-O-Sil is fine powder of amorphous silicon dioxide formed by burning silicon tetrachloride vapor in a flame of hydrogen and oxygen. In the burning process, molten SiO_2 spheres of diameters between 7 and 14 nm are formed. While cooling, these spheres collide with each other and fuse together into three dimensional chain-like aggregates which exhibit a self-similar, or fractal, structure.[18,19] The resulting fumed silica powder has a specific surface area of between 400 m^2/g and 200 m^2/g depending on the grade. For this experiment the finest grade of Cab-O-Sil, EH5 with 7 nm diameter spheres, was used.

The formation of muonium in fumed silica is interpreted as a three-stage process. First, the μ^+ stops in the SiO_2 spheres forming muonium. The fraction of muons which form muonium inside the SiO_2 spheres is assumed to be the same as the muonium production fraction in bulk silica; this fraction has been measured to be 0.61 ± 0.03.[20]

The muonium atoms next diffuse to the surface of individual spheres and emerge into the vacuum spaces between spheres. The fraction emerging from the spheres has been estimated to be (0.97 ± 0.01).[15]

The atoms then diffuse to the surface of the fumed silica layer itself in order to get out of the powder environment. Marshall[22] has calculated this rate using a diffusion equation for a model of randomly distributed spheres of radius r. The diffusion constant is:

$$D = \frac{4}{9} v r \left(\frac{\rho}{\rho'}\right) = 7.9\,\mathrm{cm}^2/\mathrm{s} \qquad (1)$$

where $\rho = 2.2$ g/cm^2 is the density of bulk silica, $\rho' = 0.032$ g/cm^2 is the density of fumed silica, and v is the mean speed of the muonium atoms. It is known from electron micrographs of the powder, however, that the powder spheres are not distributed uniformly. The tendency of the spheres to form chains with long spaces in between would increase the mean free path of a diffusing muonium atom and so increase the effective diffusion constant.

In this work an effective diffusion constant is determined by adjusting its value so that the calculated muonium yield in vacuum is in agreement with the observed yield. This experimentally determined diffusion constant is considerably larger than the previous analytical estimation and implies that the mean free path of muonium atoms in SiO_2 is roughly two orders of magnitude longer.

II. EXPERIMENTAL PROCEDURE

A. Apparatus

The apparatus used for this experiment is shown in Fig. 1(a). The TRIUMF surface muon channel, M15, delivered low-energy positive muons with a rate, limited by slits, of $\approx 6 \times 10^4$/s. The beam momentum was varied from 22 to 29 MeV/c, and had a momentum spread of either 3 or 10% (FWHM). The beam initially passed through a thin aluminized mylar mirror and a 3.8 cm diameter, 0.25 mm thick plastic scintillator. A 0.025 mm stainless steel vacuum window isolated the beam line vacuum

from the vacuum chamber, which consisted of a 15 cm stainless steel cube followed downstream by a pumping station.

The silica powder was supported by a ramp shown in side view in Fig. 1(b). The support was a frame of Al with a rectangular piece of Al foil, of typical dimensions 5.5 cm × 11 cm × 0.12 mm, stretched across it at an angle of either 60° or 66° to the vertical. The targets were made by sifting the silica powder onto the support ramp. The powder thickness was determined by weighing, and the entire target assembly was suspended approximately in the middle of the cube. The apparatus was pumped down slowly to 0.5 Torr to avoid disturbing the powder. The targets were then maintained at a pressure below 10^{-6} Torr. Typically the targets were observed for periods of days to weeks. During the longer periods settling of the powder was observed.

An attempt was made to independently estimate the non-uniformity of these powder layers. Using a solar cell and a laser, the variation in optical density was measured for two sample targets. These targets were neither pumped down from atmosphere nor suspended at an angle for any period of time. However, this test suggested that the making and handling of a target could result in a non-uniformity of 20–30% of the layer thickness over the central portion of the target.

The detection system (Fig. 1(a)) consisted of a telescope of three multiwire proportional chambers (MWPC's) with 2 dimensional readout. Following these were three plastic scintillators, labeled S and a large NaI(Tl) crystal for measuring the energy of the positrons.

The beam momentum was adjusted so that approximately half of the muons stopped in the powder and half went completely through and were lost. This was accomplished by sliding into the cube a rectangular piece of metal, called a catcher, 1.8 cm away from the target and parallel to it. The target and catcher were then imaged with the wire chamber telescope to determine the fraction of muon stops in each.

B. Data acquisition and offline analysis

In the data acquisition electronics, the triggering of the beam scintillator, T, by an incident muon, started a 8μs gate. The presence of a muon decay positron was indicated by a coincidence between the first wire chamber, all three S scintillators, and the NaI(Tl). If this sequence was not observed during the 8μs gate, the electronics were cleared and the system could accept another muon. If the decay positron sequence was observed, the coordinates of the hits in all three chambers was recorded. Also recorded was the time of the decay, as measured from the time that the incident muon triggered the beam scintillator. Events in which T fired more than once within the 8μs gate were rejected in offline analysis.

In the offline data analysis program, a straight line trajectory between the position on the three MWPC's was then calculated and extrapolated back to the center of the vertical plane containing the beam axis. A cut on χ^2 of the linear fit of wire chamber hits was imposed to ensure good track quality. A cut on the slope of the fit limits parallax uncertainties which arise when the positron trajectory is extrapolated back to the plane x=0. The trajectory was then rotated to a co-ordinate system (x, v, w)

defined so that the co-ordinate w was normal to the plane of the powder and x points along the axis of the positron counters. Table I lists different regions of space from which muon decays are observed. The mean position of the positrons seen coming from the target was defined to be at w=0. For each of these regions the time of decay was plotted; these time spectra were used for the final muonium yield determination.

Using the energy spectrum of the NaI(Tl) detector, only positrons with energies above 30 MeV were accepted. These were less likely to undergo large angle scattering at the stainless steel vacuum window preceding the wire chambers. The cut was selected so that the signal to noise ratio of the counts seen in R2 was approximately 1:1.

III. ANALYSIS

Simulation

The full experiment was simulated using the Monte Carlo program MUBEAM[23] which incorporates the diffusion model described in section IB. The simulation begins at the beam counter, where a 1 cm radius uniform density beam with a Gaussian momentum distribution is generated. As the muon passes through each material in its path its range is reduced by an amount which depends on the material's thickness and stopping power.[24] The effect of range straggling and of non-uniformities in the thickness of the powder layer was included in the simulation.

Once the simulated muons stop in the SiO_2 powder 61% are converted to muonium atoms in accordance with a μSR measurement.[20] These atoms then undergo a random walk, in the framework of a diffusion model, to get out of the powder. At the end of the random walk one of three things will occur: the muon will decay inside the target while diffusing, the muon (or muonium atom) will reach the Al substrate surface, or the muonium atom will arrive at the surface of the powder layer and be emitted into the vacuum drift space. The muonium is given a random velocity selected from a Boltzmann distribution at a temperature of 300 K, and a $\cos\theta$ angular distribution, as expected from simple geometric considerations, where θ is defined with respect to the w direction. The azimuthal distribution is assumed to be uniform. In all cases, the trajectory of the μ^+decay positron is then generated, and its intercept with the x=0 plane is histogrammed, exactly as was done for the real data. This enables the calculation of the number of vacuum muonium atoms which were not resolved with the wire chamber telescope. Comparisons between the simulated and the experimental muonium decay histograms were made in order to fix model parameters, and finally the yield was calculated from the simulation. This facilitates a direct comparison the data with a diffusion model since the effect of the beam spot width and detector resolution are included.

The validity of the $\cos\theta$ angular distribution assumption was tested by considering a histogram of the muon decays from region R2 projected along the v direction. The v-distribution of the experimental data is described by a Gaussian function of width $\sigma = 17.1 \pm 0.7$ mm. Using the simulation with a $\cos(\theta)$ distribution we find $\sigma = 16.9 \pm 0.03$ mm is predicted, while a uniform distribution has $\sigma = 18.6 \pm 0.04$ mm.

B. Stopping distribution

The stopping distribution width was measured experimentally using the catcher, which was inserted while the momentum of the beam was changed by several percent. The variation with momentum of the relative numbers of stops seen in the target and the catcher gives a measure of the stopping distribution width. Non-uniformity of the thickness of the powder layers causes an increase in the width of the muon stopping distribution in the target. The powder inhomogeneity was then adjusted in the simulation for each target to reproduce its experimental momentum scaling behavior. For the sample of targets measured, the scaling behavior implied non-uniformities of from 12 to 50% of the thickness.

C. Vacuum yield

The determination of the muonium yield was made by a comparison between the Monte Carlo simulation and the data in a region of the vacuum chamber relatively far from the target. Figure 2 shows a density plot of the number of muon decays as calculated by the extrapolation of decay positron trajectories. For each of the regions R1, R2, R3, and Target, the time of decay of the muons was plotted. These time spectra are shown in Fig. 3. The muonium signal can be seen as a nonexponential time dependence introduced by the motion of muonium into and out of the different spatial regions.

A velocity component along the w coordinate was calculated by dividing the distance of the muon decay from the target by the time of its decay. Figure 4 shows a typical velocity spectrum along with the corresponding simulation result. The good agreement indicates thermal emission.

No change in muonium yield is observed when an electric field of 2.5 V/cm was applied across the vacuum chamber, confirming the neutral nature of the signal.[16] Using a similar experimental configuration, the precession frequency of muonium in a magnetic field has also been observed.[27]

In addition to the muonium signal, however, each of the three vacuum regions contained a background from muons which stop in the target or vacuum chamber walls and are misinterpreted as coming from the vacuum. This background had a μ^+-lifetime and so could be subtracted. An experimental background test was done to determine if other sources of background were significant. Nitrogen gas, at a pressure of $\sim$1 Torr, was introduced into the vacuum chamber and additional data was taken. Because of the short mean free path in N_2, diffusion in the N_2 gas reduces the number of thermal muonium atoms reaching region R2. Other background sources, such as μ^+ stops in the walls of the chamber and the target, were not significantly affected by the presence of N_2. When the time spectra taken with N_2 in the chamber were subtracted from the vacuum data, the resulting spectra were consistent with those obtained by subtraction of an exponential background alone.

To calculate the yield of muonium, a comparison between the experimental and simulated data was made using the decay time spectrum of region R2. The spectrum was fit with a μ^+-lifetime background and the simulated muonium signal component,

with the diffusion constant in the simulation adjusted to obtain the best fit. Figure 5 shows a typical R2 timing spectrum and the resulting fit. Figure 5(a) shows both components, Fig. 5(b) shows only the background component and Fig. 5(c) shows muonium with the background subtracted.

The uncertainty in the yield due to statistical fluctuations in the data was calculated in the fitting process and ranged from 5 to 30%. The simulation contains several parameters, such as the size of the beam spot on the target and the powder inhomogeneity which were adjusted to reproduce various aspects of the data. Systematic uncertainties in the yield were determined by varying these parameters over their allowed ranges. The number of beam scintillator counts and the number of events surviving all cuts were used to normalize the Monte Carlo simulation to the data; selection of a particular normalization introduced fluctuations into the calculated yield. The systematic uncertainty in the yield was estimated to be 20%.

IV. RESULTS

A. Vacuum yields

One application for muonium is in the search for muonium conversion to antimuonium;[8] this was our primary motivation for seeking to maximize the vacuum muonium rate. This rate was obtained using powders of thickness 9.0 mg/cm^2 suspended at an angle of 66° to vertical and a beam momentum of 28.5 ± 2.85 MeV/c. Table II lists the yields measured for each target used in the antimuonium conversion experiment.

The average yield achieved was (1.9 ± 0.5) % of the incoming muons. For targets for which remained under vacuum for periods of up to 10 days, no evidence of a decrease in the yield with time was observed, although there was visual evidence of settling of the powder layer. For the muonium conversion measurement the quantitiy of interest was not the average yield, but the total amount of vacuum muonium produced over the course of the experiment. To obtain this quantity, yield measurements from individual targets were averaged weighted by the number of muons incident on that target. The total amount of muonium produced in the anti-muonium experiment was (2.4 ± 0.5) % of the incident muons. Comparable yields were obtained for both 10% and 3% momentum widths because the shape of the muon stopping distribution in the powder is dominated by the target inhomogeneity for this configuration.

The dependence of the yield on the muon stopping distribution was investigated by varying the momentum of the muon beam. These distributions are crudely characterized by the mean depth from the surface of those muons stopping in the SiO_2 . Table III lists the data including the momentum, momentum spread, and the fraction of incident muons which stopped in the target.

At a beam momentum of 22.2 MeV/c the yield per target stop for a 2.8 mg/cm^2 target was (15.9 ± 3.6)% for a narrow momentum bite and (15.0 ± 3.6)% for a wide momentum bite. The yields per incident muon were (7.6 ± 1.7)% for narrow and (5.8 ± 1.4)% for wide momentum bite. The stopping distributions in this case are less sensitive to the powder inhomogeneities, which resulted in a greater widening of the stopping distribution in thick relative to thin targets, thus decreasing the number of

muons which stop near the surface of the powder layer. These yields are consistent with previous results.[16]

The dependence of the muonium yield reaching region R2 on gas pressure has been studied. Using the thin target of 2.8 mg/cm^2, the yields were measured at N_2 gas pressures of 6 and 20 mTorr. The reduction of the number of muonium atoms decaying from region R2 is a measure of their mean free path. The cross section for scattering of muonium with N_2 molecules is related to the mean free path λ by:

$$\sigma = \frac{1}{n\lambda} \tag{2}$$

where n is the number of molecules per unit volume. λ depends on the pressure of N_2 in the vacuum chamber and was calculated from the experimental yields using the simulation. At a pressure of 6 mTorr of N_2 the cross section was found to be $\sigma = (1.3 \pm 0.2) \times 10^{-15}$ cm^{-2}, and at 20 mTorr of N_2 a value of $\sigma = (2.0 \pm 0.3) \times 10^{-15}$ cm^{-2} was obtained. For comparison, a geometric estimation of the cross section can be made using the Bohr radius of a muonium atom and the radius of a N_2 molecule, giving a value of $\sigma \sim 1.3 \times 10^{-15}$ cm^{-2}.

Yield measurements with other physical forms of SiO_2 were performed in order to better understand what properties of fumed silica allow it to produce large amounts of vacuum muonium. A suppression of the yield was observed from a fumed silica target which had been compressed,[16] indicating that the microscopic structure of a material, and not just its chemical composition, is important. Comparable yields to fumed silica were obtained from Merck Opti-Pur, an extremely pure crystalline powder of SiO_2 developed for use in the manufacture of optical fibers. While its density (0.51 g/cm^3) is much larger than that of Cab-O-Sil (0.032 g/cm^3) it has a surface area of 600 m^2/g which exceeds that of Cab-O-Sil by a factor of ~2. At a beam momentum of 28.5 MeV/c the total yields per incident muon from Opti-Pur are (1.9 ± 0.5) % for a wide momentum spread and (1.8 ± 0.4) % for a narrow momentum spread.

A form of low density SiO_2 is aerogel, a silica gel which has been dried into a solid translucent block under high gas pressures. We tested a sample with a density of 0.14 g/cm^3, and a surface area of approximately 520 m^2/g.[25] This target proved to be a poor producer of muonium, giving a yield per incident muon of only (0.7 ± 0.2) % at a beam momentum of 28.5 MeV and a 3 % momentum width. An attempt was made at cleaning the surface of the aerogel by introducing ~ 20 mTorr of O_2 into the vacuum chamber and initiating a plasma discharge. The yields after this procedure were further reduced by approximately 50 %.

From the above studies of differing forms of SiO_2 it is apparent that density or surface area alone is not sufficient to predict the muonium production capability. While, like fumed silica, aerogel is also composed of chains of silica particles of small diameters, these chains are crosslinked to produce a skeletal support for its solid form. In fumed silica the chains are entwined but not firmly connected. Another characteristic which is important for aerogel is pore size. The type of aerogel used had a nominal maximum pore size of ~20 nm. However, exposure to moisture preferentially decreases the size of the largest pores[26] by as much as a factor of 4 in some cases. The

macroscopic structure is not changed nor is the measured surface area. This could perhaps explain the reduction in yield following plasma cleaning.

B. Determination of the diffusion constant

The yield determinations in this work have been examined in the context of a diffusion model. If this model is valid, then the diffusion constant governing the emission of muonium from fumed silica should depend only on the physical characteristics of the powder structure. This means that the yields obtained for different target configurations and beam momenta should be predicted by the same diffusion constant.

While the muonium yields were well determined from the data, the diffusion constant was much more sensitive to the internal parameters of the model. The shape of the stopping distribution is especially critical. The modelling of the stopping distribution is problematic for a material like fumed silica because of the powder layer inhomogeneity.

An average inhomogeneity broadening was used for all targets of the same type when individual measurements were not available. The target inhomogeneity was the least well known for the antimuonium conversion experiment targets. For these targets, the inhomogeneity parameter in the simulation program could only be determined to approximately 18%. Varying the parameter by this amount produces a 40% change in the diffusion constant.

The procedure outlined in Sec. IIIA was used to relate the yield to a diffusion constant. Table IV show the results obtained for a variety of stopping distributions. To separate the systematic effects related to the target inhomogeneities, diffusion constants were tested for consistency separately for each target configuration using only statistical uncertainties. The χ^2 test indicates that the diffusion constants are not quite consistent for repeated measurements at different momenta on the same target, but this could mean that the systematic errors are on the order of the statistics. Figure 6 shows a plot of these diffusion constants as a function of the mean stopping depth in the powder. The error bars plotted include both the statistical and systematic uncertainties. There are no obvious trends.

The weighted mean of the average diffusion constants for each target was then calculated. The resulting effective diffusion constant, including systematic uncertainties, was (525 ± 100) cm^2/s. The value of $\chi^2_\nu = 1.3$ for the fit indicates the diffusion constants of different target configurations were consistent.

Recently Woodle *et al.*[27] measured the yield of thermal muonium from fumed silica at an incident beam momentum of 20.1 MeV/c and width of 1.5 MeV/c. The target thickness was 9.0 mg/cm^2. Yields of (18 ± 2)% of the stopped muons and (11 ± 2)% of the incoming muons were obtained. The diffusion constant was calculated to be (1068 ± 81) cm^2/s, although details of the model are not given. The apparatus used was similar but this data cannot be directly compared with our experiment. To make a comparison, our Monte Carlo simulation was run using the diffusion constant inferred from this work, 525 ± 100 cm^2/s, in the configuration of the PSI experiment. When the target was assumed to be perfectly homogeneous the

simulated yields calculated were (6.6 ± 0.4)% of the incident muons, or (17 ± 1)% of the stops in the silica. If, however, the targets were assumed to have an inhomogeneity of 30% of the target thickness, comparable to the targets used in this work, the simulated yields were (4.9 ± 0.3)% of the incident muons, or (9.9 ± 0.6)% of the stops in the silica. Thus it would appear that the targets used by Woodle *et al.* exhibited a larger diffusion constant, and also that there are discrepancies in the modelling of the stopping distribution. The variation in the simulated yields gives an indication of the importance of the target inhomogeneity in the modelling of the stopping distribution in the target.

V. CONCLUSIONS

In this work we report on various aspects of muonium production from silica. It was found that the selection of an appropriate material depends not only on surface area and density but also on the microscopic structure of the particular form of silica. The muonium thus produced is emitted with thermal velocities into vacuum and with an angular distribution consistent with $\cos\theta$.

The emission of muonium from fumed silica was determined to be generally consistent with a diffusion model. Previous work[16] had noted inconsistencies in the diffusion constants for different target thicknesses and muon beam configurations. A more consistent description was possible when the inhomogeneity in the thickness of the powder layer was included in the calculation of the stopping distribution in the target. Production of targets of consistently high quality remains a problem.

The diffusion constant obtained is an effective value describing the different processes in fumed silica which are involved in the production of muonium. This value is substantially larger than that suggested by an analytical calculation assuming a uniform distribution of spheres of silica. This is interpreted as an increase in the mean free path of the muonium atoms due to the arrangement of the SiO_2 spheres, and indicates that the microscopic structure of the production material must be considered when explaining muonium diffusion.

ACKNOWLEDGEMENTS

We wish to acknowledge the contributions of Mr. Zev Gelbart, Mr. Peter Vincent, Mr. Keith St. Lawrence, Dr. Jack Beveridge, and the TRIUMF cyclotron staff. Financial support for this work was provided by grants from the Natural Sciences and Engineering Research Council of Canada and the US National Science Foundation and Department of Energy.

References

*Present address: Carleton University, Ottawa, Ontario, Canada K1A 0R1.
†Present address: TRIUMF, Vancouver, British Columbia, Canada V6T 2A3.
‡Present address: National Laboratory for High Energy Physics (KEK), Ibaraki 305, Japan.
§Present address: Gustavus Adolphus College, St. Peter, Minnesota 56082.

**Present address: University of California (Irvine), Irvine, CA 92717.
††Present address: University of Arizona, Tucson, Arizona 85721.
§§Deceased.

[1]V.W. Hughes and T. Kinoshita, in *Muon Physics*, edited by V.W. Hughes and C.S. Wu (Academic, New York, 1977) Vol. 1.
[2]F.G. Mariam *et al.*, Phys. Rev. Lett. **49**, 993 (1982).
[3]D.E. Casperson *et al.*, Phys. Rev. Lett. **38**, 956 (1977).
[4]C.J. Oram *et al.*, Phys. Rev. Lett. **52**, 910 (1984).
[5]A. Badertscher *et al.*, Phys. Rev. Lett. **52**, 914 (1984).
[6]S. Chu *et al.*, Phys. Rev. Lett. **60**, 101 (1988).
[7]B. Ni *et al.*, Phys. Rev. Lett. **59**, 2716 (1987).
[8]T.M. Huber *et al.*, Phys. Rev. Lett. **61**, 2189 (1988);
T.M Huber *et al.*, submitted to Phys. Rev. D.
[9]V.W. Hughes *et al.*, Phys. Rev. **A5**, 63 (1960).
[10]B.A. Barnett *et al.*, Phys. Rev. A **11**, 39 (1975).
[11]P.R. Bolton *et al.*, Phys. Rev. Lett. **47**, 1441 (1981).
[12]C.J. Oram, C.A. Fry, J.B. Warren, R.F. Kiefl and J.H. Brewer, J. Phys. **B 14**, L789 (1981).
[13]K.R. Kendall, Ph.D. thesis, University of Arizona, 1972 (unpublished).
[14]A.P. Mills, Jr. *et al.*, Phys. Rev. Lett. **56**, 1463 (1986).
[15]G.M. Marshall *et al.*, Phys. Lett. **65A**, 351 (1978).
[16]G.A. Beer *et al.*, Phys. Rev. Lett. **57**, 671 (1986).
[17]Technical report available from Cabot Corporation, 125 High Street, Boston, MA 02110, USA.
[18]B. Mandelbrot, *Fractals, Form, Chance, and Dimension* (Freeman, San Francisco, 1977).
[19]T.A. Witten, Jr. and L.M. Sander, Phys. Rev. Lett. **47**, 1400 (1981).
[20]R. Kiefl *et al.* Hyperfine Interactions **6**, 185 (1979).
[21]G.M. Marshall, J.B. Warren, C.J. Oram, and R. F. Keifl, Phys. Rev. D **25**, 1174 (1982).
[22]G.M. Marshall, Ph.D. thesis, University of British Columbia, 1981 (unpublished).
[23]Further details are given in A.C. Janissen, M. Sc. Thesis, University of Victoria, 1989, and A.C. Janissen, Victoria Physics Note 89-1.
[24]J.F. Janni, Atomic Data and Nuclear Data Tables **27**, 341 (1982).
[25]C.A.M. Mulder and J.G. van Lierop, Aerogels, J. Fricke ed. (Springer-Verlag, Berlin, 1985), p. 68.
[26]G. Schuck and W. Dietrich, Aerogels, J. Fricke ed. (Springer-Verlag, Berlin, 1985), p. 148.
[27]K.A. Woodle *et al.*, Z. Phys. **D9**, 59-64 (1988).

TABLE I. Definitions of the drift regions of the vacuum system where w and v are the co-ordinates of the position of the muon decay. (See Fig. 2)

Region	Condition on w (mm)	Condition on v (mm)
Target	$-5 \leq w < 5$	$-50 \leq v \leq 50$
R1	$5 \leq w < 15$	$-50 \leq v \leq 50$
R2	$15 \leq w < 25$	$-50 \leq v \leq 50$
R3	$25 \leq w < 35$	$-50 \leq v \leq 50$
R4	$35 \leq w < 45$	$-50 \leq v \leq 50$

TABLE II. Yields for targets used in the muonium conversion experiment in both 1987 and 1988 runs.

Run	Target number	SiO_2 mg/cm^2	$\frac{\Delta P}{P}$ %	Yield / tgt stop %	Yield / inc. μ^+ %
115	1987-1	8.5	10	4.2 ± 1.0	2.4 ± 0.6
116	1987-1	8.5	10	2.6 ± 0.7	1.5 ± 0.4
117	1987-1	8.5	10	3.8 ± 1.0	2.2 ± 0.6
118	1987-1	8.5	10	3.8 ± 0.9	2.2 ± 0.5
119	1987-1	8.5	3	4.3 ± 1.1	2.2 ± 0.6
120	1987-1	8.5	3	4.4 ± 1.2	2.3 ± 0.6
314	1988-1	9.1	3	5.3 ± 1.3	2.5 ± 0.6
315	1988-1	9.1	3	2.3 ± 0.9	1.1 ± 0.4
348	1988-1	9.1	10	4.8 ± 1.1	2.6 ± 0.6
362	1988-2	8.7	10	4.5 ± 1.1	2.5 ± 0.6
369	1988-2	8.7	10	2.3 ± 0.6	1.2 ± 0.3
370	1988-2	8.7	10	2.6 ± 0.7	1.4 ± 0.4
387	1988-3	8.3	10	3.8 ± 0.9	2.1 ± 0.5
406	1988-4	8.4	3	5.2 ± 1.2	2.5 ± 0.6
441	1988-4	8.4	3	4.3 ± 1.0	2.0 ± 0.5
407	1988-4	8.4	10	4.5 ± 1.1	2.4 ± 0.6
442	1988-4	8.4	10	5.9 ± 1.6	3.2 ± 0.9
443	1988-4	8.4	10	5.1 ± 1.3	2.8 ± 0.7

TABLE III. Yields obtained with beam momentum scans on two targets to probe the yield as a function of stopping depth in the powder. Included is the fraction of incident muons which stop in the target at specific momenta as calculated by the Monte Carlo.

Run	SiO_2 mg/cm^2	P MeV/c	$\frac{\Delta P}{P}$ %	Fr. in Target	Yield / tgt stop %	Yield / inc. μ^+ %
72	13	24.3	10	0.56	7.5 ± 1.9	4.1 ± 1.0
79	13	24.3	3	0.56	7.9 ± 1.9	4.4 ± 1.1
80	13	23.8	3	0.67	6.2 ± 1.7	4.2 ± 1.1
87	13	23.2	3	0.80	2.9 ± 0.8	2.3 ± 0.7
82	13	22.6	3	0.90	1.5 ± 0.5	1.3 ± 0.5
86	13	21.8	3	0.96	0.5 ± 0.5	0.4 ± 0.4
458	17.9	28.2	10	0.51	4.5 ± 1.0	2.4 ± 0.6
459	17.9	28.2	3	0.51	7.4 ± 1.7	3.7 ± 0.8
460	17.9	27.9	3	0.61	6.5 ± 1.5	4.0 ± 0.9
461	17.9	27.6	3	0.71	5.1 ± 1.2	3.6 ± 0.8

TABLE IV. Different target configurations and incident muon beam momenta for which yield data was taken and the diffusion constant determined. Errors assigned to the weighted mean rows include both statistical and systematic uncertainties.

Run	P MeV/c	$\frac{\Delta P}{P}$ %	Mean Depth (mm)	D cm^2/s	$+\Delta D$ / $-\Delta D$ Statistical cm^2/s	Dev'n from Mean σ
72	24.3	10	0.51	1600	340 / 310	1.2
79	24.3	3	0.28	1390	250 / 220	0.5
80	23.8	3	0.53	1470	410 / 360	0.6
87	23.2	3	0.90	870	390 / 320	1.0
82	22.6	3	1.34	840	420 / 350	1.3
Weighted mean and total error				1250	420	
148	22.0	3	0.45	370	40 / 40	
149	22.0	10	0.50	440	100 / 90	
Weighted mean and total error				380	150	
458	28.2	10	2.54	840	70 / 70	2.1
459	28.2	3	1.78	1020	130 / 130	0.2
460	27.9	3	2.01	1160	90 / 90	1.9
461	27.6	3	2.29	1220	170 / 160	1.3
Weighted mean and total error				990	450	

Figure captions

1. Schematic diagram of the apparatus to measure muonium yields. Dashed lines represent stainless steel vacuum windows. Insert: Side view of the target holder.
2. Density plot of position of muon decays in space along with definitions of regions TGT, R1, R2, and R3. Yield was determined on the basis of analysis of region R2.
3. Muon decay times for various spatial regions.
4. Velocity distribution of events from spatial regions R1, R2, and R3 for the powder and the Monte Carlo simulation.
5. Muon decay times for events in region R2. The points represent data and the histogram indicates the yield fit including simulated muonium and background: (a) all events, (b) histogram shows only the background from target decays, (c) data and final yield fit after subtracting the background shown in (b).
6. Diffusion constants for all yield measurements plotted against the mean muon depth of the stopping muons.

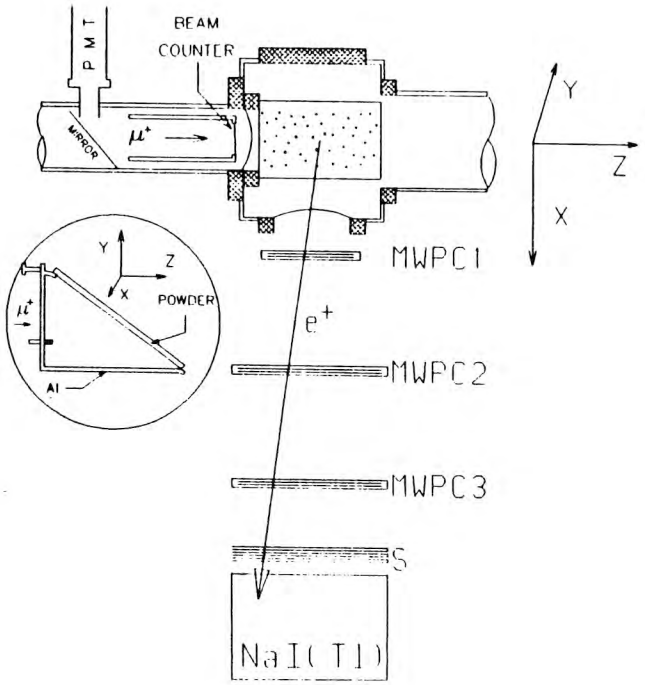

Fig. 1

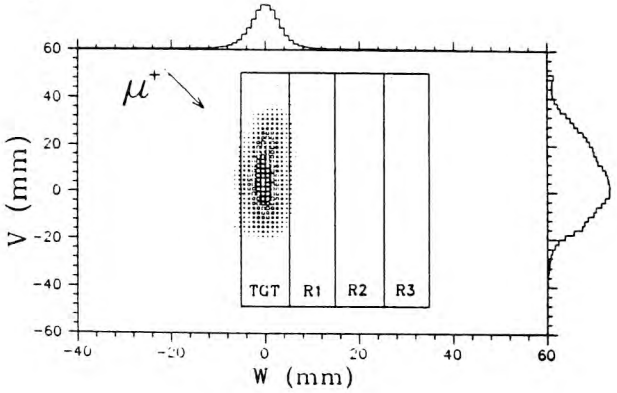

Fig. 2

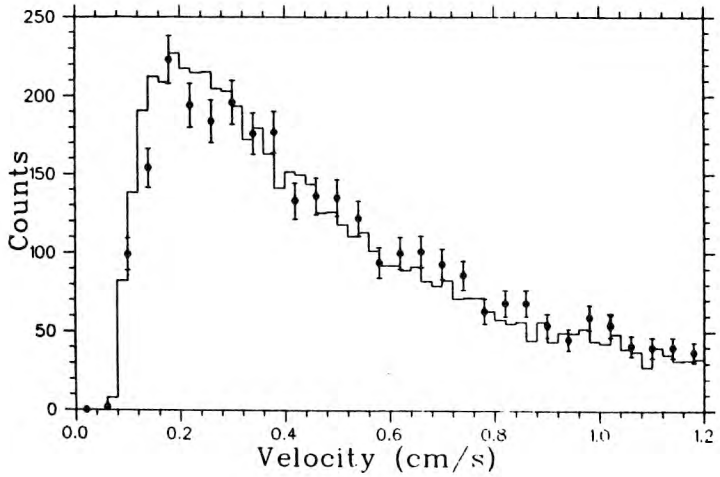

Fig. 4

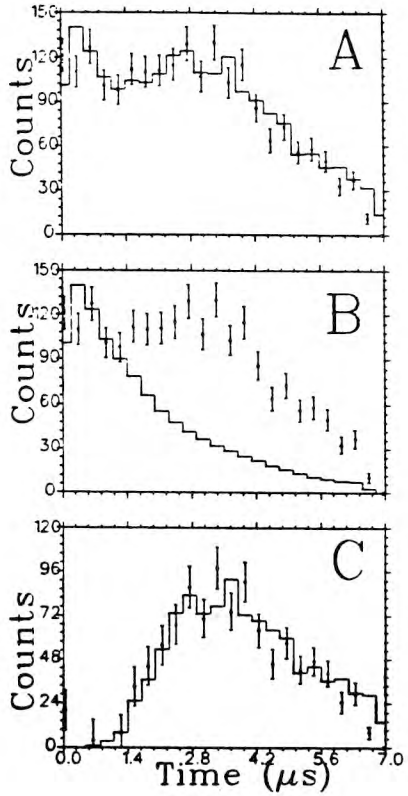

Fig. 5

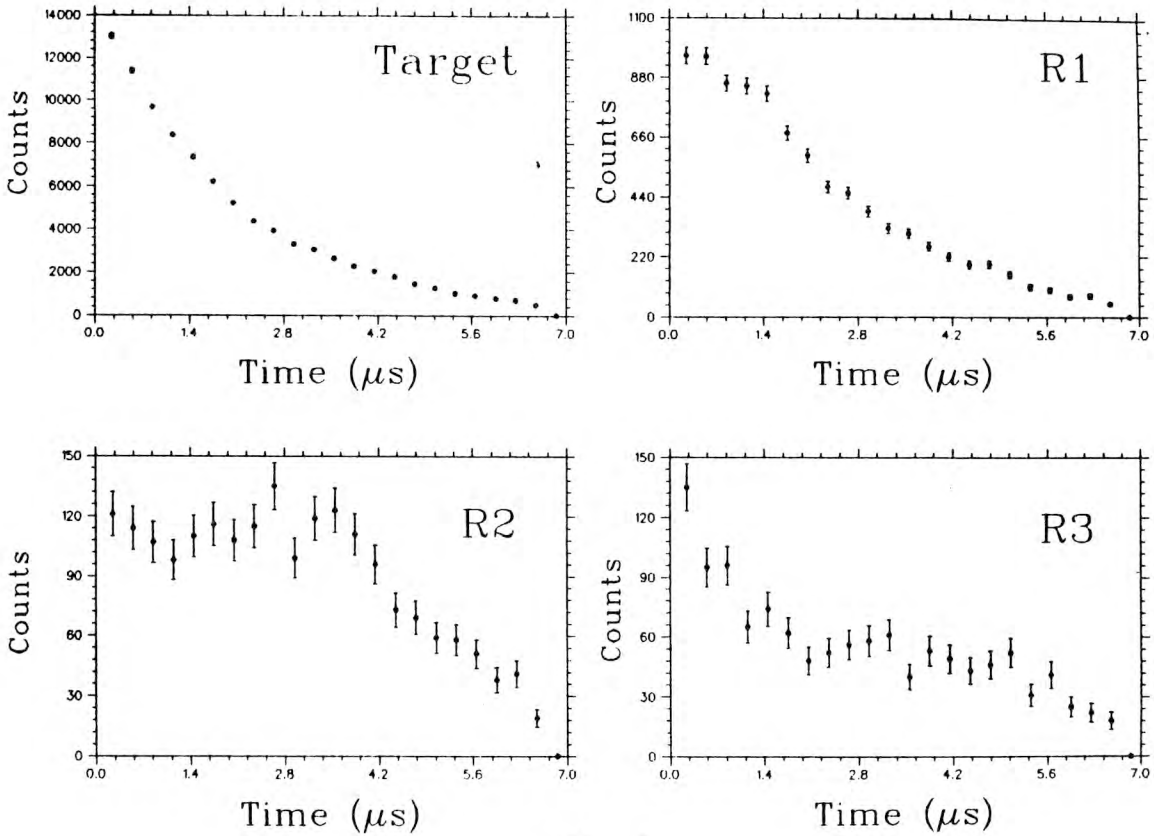

Fig. 3

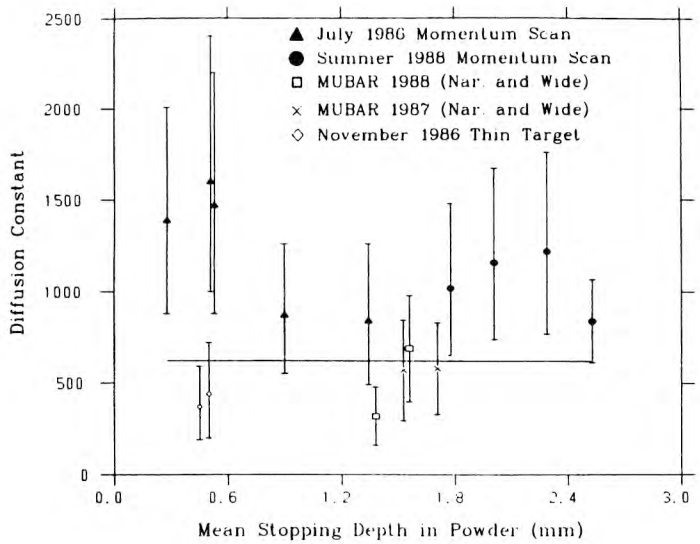

Fig. 6